The dynamic indentation behavior of steel at large depths of penetration

G. Sundararajan[a)] and S.N. Dikshit
International Advanced Research Centre for Powder Metallurgy and New Materials, Hyderabad-500005, India

(Received 24 July 2008; accepted 15 September 2008)

The objective of the present study is to investigate the dynamic indentation behavior of steel plate material when impacted by ogive-shaped projectiles and in particular under indentation conditions involving large depths of penetration (i.e., depth of penetration greater than projectile radius). Toward the above purpose, dynamic indentation of steel plates of thickness 20, 40, and 80 mm have been carried out using projectiles of diameter 6.2 and 20 mm, and over a range of impact velocities so as to attain depths of penetration in the range 1.4 to 3.6 times the projectile radius. The results indicate that the dynamic hardness, the plastic zone size, specific energy consumed in plastic deformation within the plastic zone, and the average plastic strain within the plastic zone increases continuously with increasing values of depth of penetration normalized by projectile radius. Certain subtle differences regarding the nature of plastic deformation between indentation at large and shallow depths of penetration are presented. However, on a macroscopic scale, the indentation mechanisms and processes are broadly similar and show continuity in terms of behavior across the whole penetration depth range.

I. INTRODUCTION

The dynamic indentation behavior of metals and alloys, including steels, have been evaluated by numerous investigators with the main purpose of determining their dynamic hardness value in relation to their static hardness value.[1–6] Tabor[1] carried out pioneering work in this area by determining the strain rate sensitivity of pure metals through simple impact experiments with spherical balls (at terminal velocities < 1 m/s). Mok and Duffy[2] carried out impact experiments in the velocity range 0.04–6 m/s on four metallic materials with a hard spherical ball and thereby obtained the dynamic flow stress–mean plastic strain data using the well-known relationships between hardness and flow stress and indentation diameter and plastic strain as originally proposed by Tabor.[1] Sundararajan and Shewmon[3] extended the work of Mok et al.[2] to higher impact velocities (20 to 250 m/s) and obtained the variation of dynamic flow stress with mean plastic strain in the case of a large number of metals and alloys. In particular, these authors noted that the strain rate sensitivity (defined as the ratio of dynamic to static hardness at the same mean plastic strain) was the highest for pure metals and stainless steels and the lowest for Cu–Be, TD nickel, and Al7075 alloy.

Tirupataiah and Sundararajan[4] have subsequently analyzed the dynamic hardness/flow stress versus mean plastic strain data in the case of pure copper and iron. They concluded that beyond a critical mean strain the deformation beneath the indentor becomes localized, triggered by the softening of the material because of the temperature rise in the plastic zone. The mechanics of localization were analyzed recently and in great detail by Sundararajan and Tirupataiah.[7,8] In a recent article concerned with the dynamic hardness measurements using a dropped ball, Clough et al.[9] have also observed ballistic softening of hardness/yield stress beyond a critical strain consistent with the observations of Tirupataiah and Sundararajan.[4] The dynamic indentation hardness and rate sensitivity of a wide range of metals and alloys have been obtained by Subhash and co-workers[5,6] using a dynamic Vickers indentation test. Their results also indicate that the ratio of dynamic Vickers hardness to the dynamic flow stress at 8% plastic strain (also called the constraint factor) is around 2.875 and similar to the value of 3.0 obtained under static indentation conditions.

A uniform feature of all the results discussed earlier is that they all pertain to data obtained under shallow penetration conditions, i.e., the depth of penetration is lower than the radius of indentation. In contrast, under actual ballistic test conditions, the depth of penetration is

[a)]Address all correspondence to this author.
e-mail: gsundar@arci.res.in
This author was an editor of this focus issue during the review and decision stage. For the *JMR* policy on review and publication of manuscripts authored by editors, please refer to http://www.mrs.org/jmr_policy
DOI: 10.1557/JMR.2009.0090

invariably larger than the indentation/crater radius. It should be interesting to study the dynamic indentation behavior at such high penetration depths to see whether the concepts pertinent to shallow indentation experiments are equally valid under higher depths of penetration.

However, it needs to be noted that the dynamic indentation to high depths (as in ballistic tests) involves extensive and gross plastic deformation of the material being indented. As a result, indentation under the above conditions occurs in the fully plastic indentation regime. Under fully plastic indentation conditions at shallow penetration depths the constraint factor, which is defined as the ratio of hardness to the flow stress of the material being indented at the same mean strain and the normalized plastic zone size (defined as the ratio of plastic zone radius to that of the indentation radius), lie in the range 2.8–3.0 and more importantly, are independent of the mean plastic strain. The fully plastic indentation regime is also characterized by a plastic zone beneath the indentor (or projectile) confined in all directions by an elastic/rigid region except for being open to the front face of the sample, as illustrated in Figs. 1(a) and 1(b). In this figure, the arrows indicate the direction of material flow. It also follows that once the plastic zone touches the back-face of the sample/plate, as illustrated in Fig. 1(c), the plastic zone is no longer confined, and this causes the material to switch its direction of flow toward the back face of the sample/plate. This, in turn, leads to stretching and bending of the sample material in front of the indentor/projectile and ultimately causes a bulge on the back face, as illustrated in Fig. 1(c). Thus, deformation conditions pertinent to the indentation process, i.e., constrained, plane strain plastic flow, are obtained during the ballistic penetration only when the plastic zone is confined to well within the back face of the sample/plate. The ballistic penetration data, which satisfies the previous condition, will only be considered in this article.

In the present study, steel samples of varying thickness (20, 40, and 80 mm) have been impacted by ogive-shaped projectiles of different diameters (6.2 and 20 mm) over a range of velocities to obtain depths of penetration in the range of 1.4–3.6 times the projectile radius. The dynamic hardness obtained and the normalized plastic zone size measured from the previous experiments will be presented and discussed in terms of the applicability of "fully plastic" indentation models validated for shallow depth of penetration to the present results.

II. EXPERIMENTAL DETAILS

A. Plate material

Rolled homogeneous armour (RHA) plates of thicknesses 20, 40, and 80 mm were used as the test material. The mechanical properties of these plates are presented in Table I. The Vickers hardness (HV) values reported in Table I were determined at a load of 30 Kg. The tensile properties of the RHA plates (i.e., the yield strength, the ultimate tensile strength, uniform strain, and the fracture strain) were obtained from the load-sample extension data obtained by tensile testing of specimens machined from the RHA plates, and the resulting data is provided in Table I. The true plastic flow stress (σ)–true plastic strain (ε) obtained from load-extension data were fitted to an equation of the form,

$$\sigma = K\varepsilon^n \quad . \tag{1}$$

In Eq. (1), K is the strength coefficient and n is the strain-hardening exponent. The best-fit values of K and n are listed in Table I. Although the chemical compositions of the RHA plates are identical irrespective of plate thickness, their hardness values are different primarily because of decreasing cooling rates (after heat treatment) associated with thicker plates.

B. Projectile

Steel projectiles with an ogive nose but having diameters of 6.2 and 20 mm (beyond the nose region) and masses of 5.2 and 110 g, respectively, were used in the

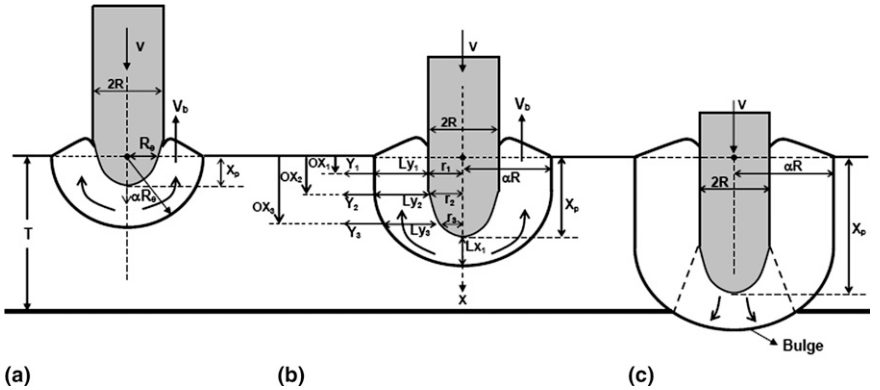

FIG. 1. A schematic view of the penetration of an ogive projectile of radius R up to various depths into a steel plate of thickness T. The various symbols in these figures are explained in the text.

TABLE I. The mechanical properties of the steel plates.

Property	Units	Value		
		20-mm plate	40-mm plate	80-mm plate
1. Vickers hardness (30-Kg load)	Kg/mm^2	350 ± 10	315 ± 10	295 ± 10
2. Projected area hardness (PAH)[a]	MPa	3730	3357	3144
3. Yield strength[b]	MPa	1080	920	860
4. Ultimate tensile strength[b]	MPa	1160	1000	960
5. Uniform strain[b]	Percent	5.0	6.5	7.0
6. Fracture strain[b]	Percent	15.0	17.0	19.0
7. Strength coefficient (K)[c]	MPa	1500	1400	1285
8. Strain-hardening exponent (n)[c]	...	0.070	0.087	0.100

[a]PAH = (HV/0.92).9.806.
[b]Tensile test carried out at a crosshead speed of 20 mm/min corresponding to an average strain rate of 1.33×10^{-1}/s.
[c]Best-fit values obtained using the relation, $\sigma = K\varepsilon^n$.

dynamic indentation tests. The hardness of the projectile (HV 750 and 640 at 30 Kg load for projectile of diameters of 6.2 and 20 mm, respectively) is more than a factor of two higher than the steel plate used in the present experiments. The three-dimensional profile of the projectile, including that of the nose, was determined using a three-dimensional profile measuring machine.

C. Indentation test details

All the dynamic indentations were carried out at zero obliquity. The sizes of the plates were approximately 1 m × 1 m irrespective of the plate thickness. During the test, the steel plates were firmly clamped to the holder and kept at a distance of about 30 m from the gun. The projectile velocity was measured by placing two screens of aluminum foils (connected electrically to a digital chronometer) in the path of the projectile as described elsewhere.[10] The accuracy of velocity measurement was within ±5 m/s. It was ensured during the test that the indentations formed by impact were separated by at least 4 diameters of the projectile and also at least by 2 diameters from the edges of the plate. In the present set of experiments involving annealed steel plates of low hardness, the rebound of the projectiles subsequent to the penetration process was minimal with the projectile just falling down at distances less than one foot in front of the plate. Thus, the rebound velocity and rebound energy of the projectile can be safely neglected.

D. Post-indentation examination

After the dynamic indentation tests, the depth of penetration (X_p, Fig. 1) was measured using an electronic digital caliper (±0.1 mm accuracy), the entry hole diameter [2 R_e; Fig. 1(a)] also using a digital caliper and the indentation volume (U) by filling up the crater (up to the original plate surface level) with plasticene of known density.

Subsequently, selected indents were sectioned along their diameter to result in a sectioned surface, as illustrated in Figs. 1(a) and 1(b). The sectioned surface was then ground and polished with emery paper up to 600 grits. Microhardness measurements (at 500 g load) were performed at regular intervals on the sectioned surface along the lines Y_1, Y_2, Y_3, and X_1, as shown in Fig. 1(b). Using the previous data, the hardness-distance profile could be determined and in turn the distance up to which the plastic zone extends from the side walls of the indentation (Y_1, Y_2, Y_3) and also below the tip of the indentation (i.e., along X direction).

III. EXPERIMENTAL RESULTS

A. Choice of experiment data

As mentioned in Sec. I, the main objective of the present study is to investigate the indentation behavior of steel at large depths of penetration. Indentation by definition refers to material deformation under plane strain; constrained conditions wherein the plastic zone ahead of the penetrating projectile is confined and does not impinge on the back face of the steel plate (see Fig. 1). Dynamic indentation experiments were carried out using various combinations of plate thickness and projectile diameters.[11] Initiation of the bulge on the backside of the steel plate provided the clearest indication that the plastic zone ahead of the projectile had impinged on the back face of the steel plate. On the basis of such a criterion, it was concluded that the plastic zone was confined within the plate thickness over a reasonably large range of impact velocities for 6.2-mm projectile striking 20-mm plate (V = 300 to 650 m/s), 20-mm projectile striking 40-mm plate (V = 290 to 600 m/s), and 20-mm projectile striking 80-mm plate (V = 280 to 800 m/s). The experimental data, from the three projectile/plate combinations mentioned previously, will be presented and discussed in this article.

B. Depth and volume of penetration and dynamic hardness (H_d)

Typical sectioned views of the indentations formed on 80-mm-thick plate and 20-mm plate are presented in Figs. 2(a)–2(d). The indentations faithfully reproduce the original projectile shape leading us to conclude that the projectile has not suffered any permanent deformation. It is also clear from Fig. 2 that the indentations are well confined within the plate material because no bulge exists on the back face of the plates.

The variation of the depth of penetration (X_p) and the indentation volume (U) with impact velocity is illustrated for 6.2-mm projectile striking 20-mm plate, 20-mm projectile striking 40-mm plate, and 20-mm projectile striking 80-mm plate in Figs. 3, 4, and 5, respectively. In all cases, both X_p and U increase continuously with increasing impact velocity (V).

Because the volume of the indentation formed (U) is for a given kinetic energy of the projectile, the dynamic indentation hardness (H_d) can be simply calculated as

$$H_d = \tfrac{1}{2}mV^2/U \quad . \tag{2}$$

The variation of H_d calculated in the previous manner and normalized by the static hardness (H; see Table I), as a function of the depth of penetration (X_p), is presented in Figs. 6(a), 6(b), and 6(c) for 6.2-mm projectile on 20-mm plate, 20-mm projectile on 40-mm plate, and 20-mm projectile on 80-mm plate, respectively. In all cases, the normalized hardness (H_d/H) does increase with increasing penetration. However, the rate of increase of H_d/H with increasing penetration appears to decrease at higher X_p values in the case of 6.2-mm projectile on 20-mm plate and 20-mm projectile on 40-mm plate. In contrast, for 20-mm projectile on 80-mm plate, the normalized hardness (H_d/H) appears to increase at a higher rate at higher depths of penetration [see Fig. 6(c)].

It is also clear from Figs. 6(a)–6(c) that the dynamic hardness, while being close to the static hardness at the lowest penetration depths, increases substantially with increasing penetration leading to the dynamic hardness being 15% to 50% higher than the static hardness at larger depths of penetration. This aspect will be discussed in detail in Sec. IV.

C. Plastic zone size

As illustrated in Fig. 1, the indentation formed by the projectile is surrounded by a plastic zone. The size of the plastic zone can be easily determined by carrying out microhardness tests on sectioned surfaces at regular spacing along Y_1, Y_2, Y_3, and X_1 directions, as illustrated in Fig. 1(b). The distance at which the microhardness value reaches the base value (i.e., distance L_{y1}, L_{y2}, L_{y3}, and L_{x1} in Fig. 1) can then be used to obtain the normalized plastic zone size (α) at different distances from plate top surface as

$$\alpha = \frac{L_{y1} + r_1}{r_1} = \frac{L_{y2} + r_2}{r_2} = \frac{L_{y3} + r_3}{r_3} \quad . \tag{3}$$

Typical microhardness profiles obtained on the sectioned surfaces of indentations are illustrated in Figs. 7 and 8. The microhardness profiles pertaining to indentations formed when a 6.2-mm-diameter projectile impacts a 20-mm plate are provided in Fig. 7. For an impact velocity of 404 m/s [Figs. 7(a) and 7(b)], the size of the plastic zone (L_{y1} and L_{y2}) is around 4.75 mm independent of the location of the profile and this corresponds to a value of 2.7 for α. In the case of indentation formed at a velocity of 645 m/s [see Fig. 7(c)], the plastic zone size is 6.2 mm and hence the α value is 3.

Further examples of experimentally obtained microhardness profiles formed by the impact of 20-mm projectiles on 80 and 40 mm are presented in Figs. 8(a) and 8(b), respectively. In these cases, α values of 2.7 and 2.42 have been obtained. Microhardness profiles were obtained on many other indentations. In all cases, the α value was the same irrespective of the location at which the microhardness profile was carried out and also when the microhardness value was carried out beneath the bottom of the indentor. Thus, it is clear that the plastic zone shape is hemispherical when the penetration depth is lower than the nose length of the projectile and in contrast has a shape of a cylinder with a hemispherical bottom when the penetration depth exceeds the nose length of the projectile. This is schematically illustrated in Fig. 1.

The value of α was measured on the basis of microhardness profiles performed on sectioned surfaces in the case of 10 different indentations. The resulting data on α as a function of depth of penetration is presented in Fig. 9. It is clear that the α values are increasing continuously with increasing penetration. More importantly, the α values are substantially higher in the case of indentations formed by 6.2-mm projectiles impacting 20-mm-thick plate as compared to 20-mm projectiles impacting 40 or 80-mm-thick plates.

IV. DISCUSSION

In this section, the results presented in the last section will be analyzed with a view to understand the nature of deformation during the indentation process to depths higher than normally encountered during hardness tests.

A. Energy consumed in plastic deformation

In the present study, we are concerned with the dynamic indentation of steel plates by ogive projectiles; therefore, it is important that almost all of the kinetic energy of the impacting projectile is consumed in the form of plastic deformation within the constrained

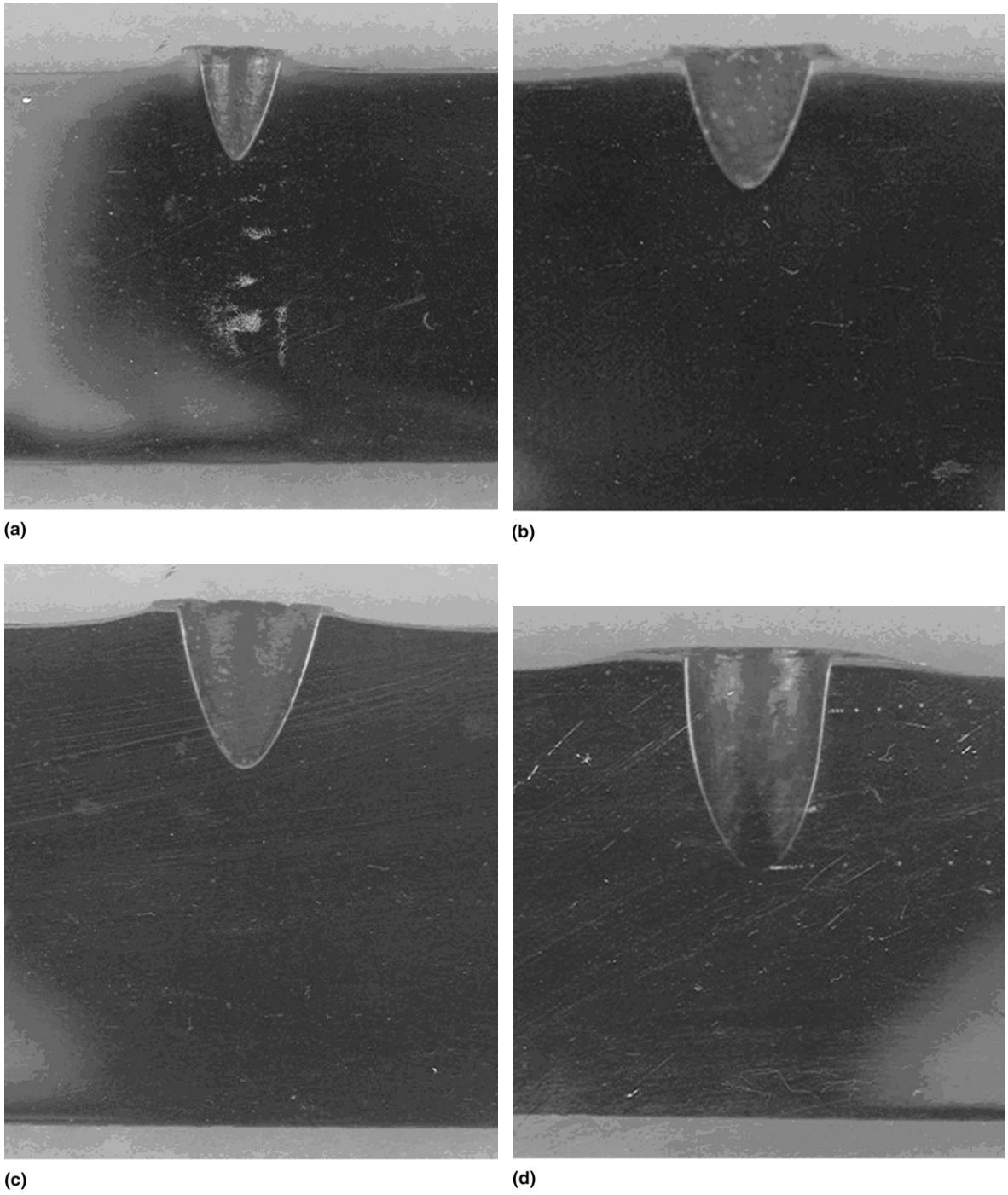

FIG. 2. The sectioned views of the impact craters formed on a 20-mm-thick steel plate by 6.2 mm diameter at impact velocities of (a) 202, (b) 363, (c) 404 m/s, and (d) 645 m/s.

plastic zone formed in the steel plate surrounding the penetrating projectile. Only under the previous conditions, the indentation resistance is a measure of the dynamic hardness of the steel plate material. In an earlier study,[12] it was demonstrated that the projectile do not suffer any permanent plastic deformation under the experimental conditions used in this study. Similarly, it was demonstrated that the energy expended in the elastic deformation of the steel plate and projectile and also the energy lost in the form of propagation of stress waves away from the impact site are negligible compared to the input kinetic energy for the projectiles and velocities relevant to the present investigation.[4] Finally, a detailed numerical analysis of the projectile

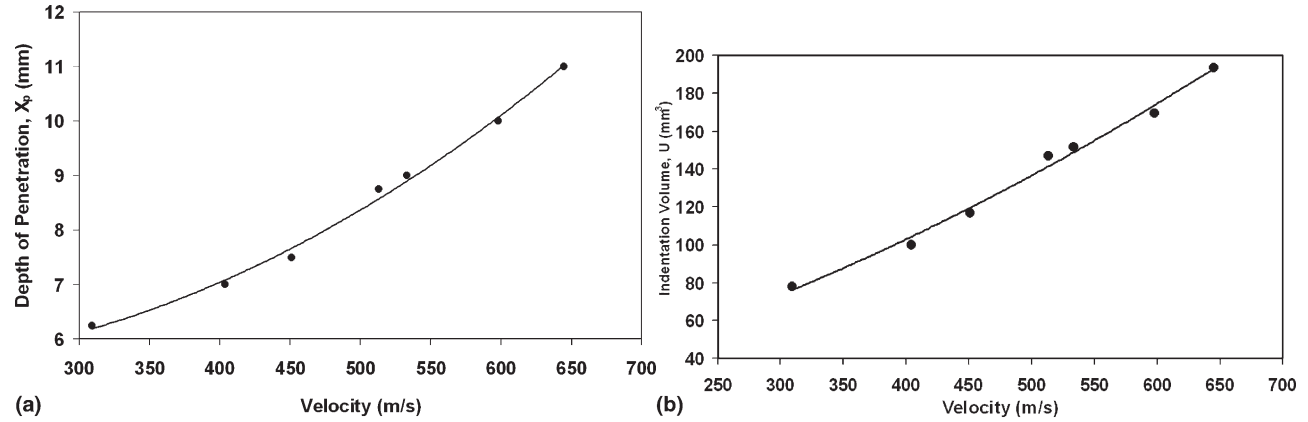

FIG. 3. The variation of (a) depth of penetration (X_p) and (b) identation volume (U) with impact velocity for a 6.2-mm-diameter projectile impacting a 20-mm-thick steel plate.

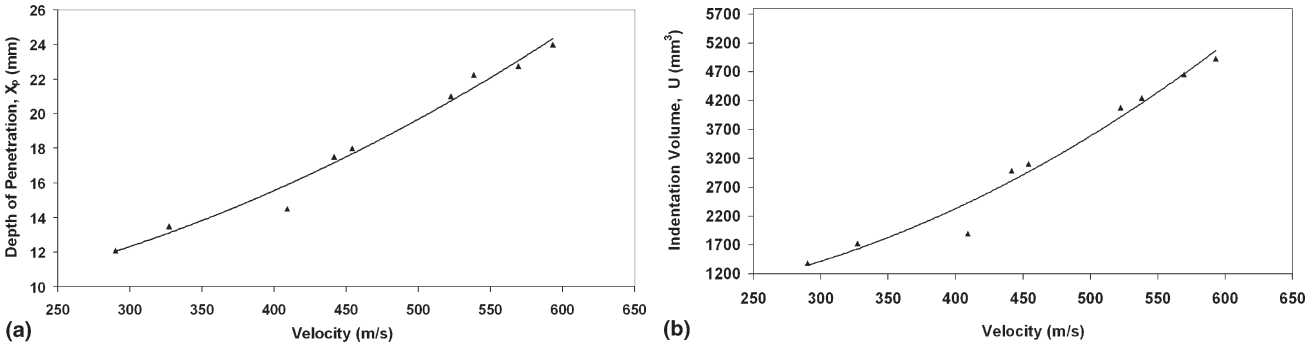

FIG. 4. The variation of (a) depth of penetration (X_p) and (b) indentation volume (U) with impact velocity for a 20-mm-diameter projectile impacting a 40-mm-thick steel plate.

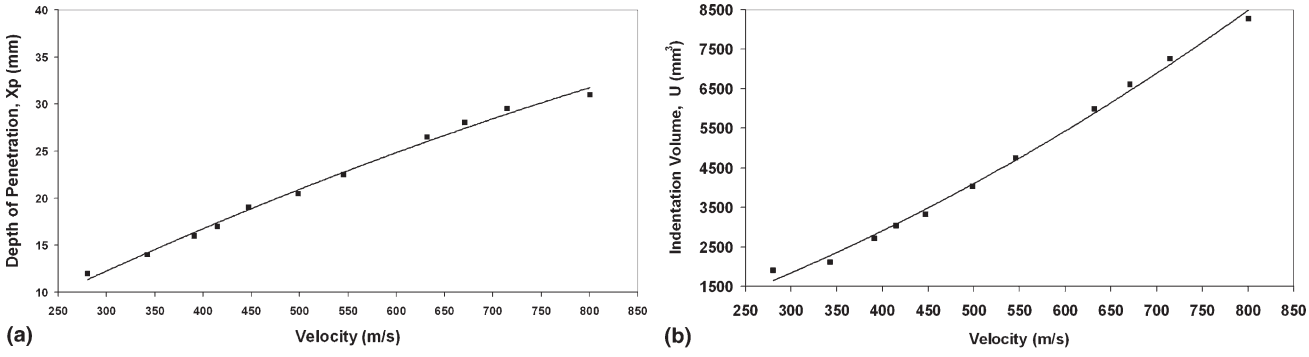

FIG. 5. The variation of (a) depth of penetration (X_p) and (b) indentation volume (U) with impact velocity for a 20-mm-diameter projectile impacting a 80-mm-thick steel plate.

penetration[12] has also shown that the energy consumed at the interface between the projectile and the indentation wall, because of the presence of friction, is negligible in the velocities of interest to the present study.

Inertial energy represents the energy required to displace the plate material away from the path of the penetrating projectile. Such a material displacement occurs first in the radial direction and then backwards, as shown by the curved arrows in Fig. 1. The velocity, V_b, with which the plate material moves backwards, can be easily determined by imposing the condition of conservation of mass flow rate to give

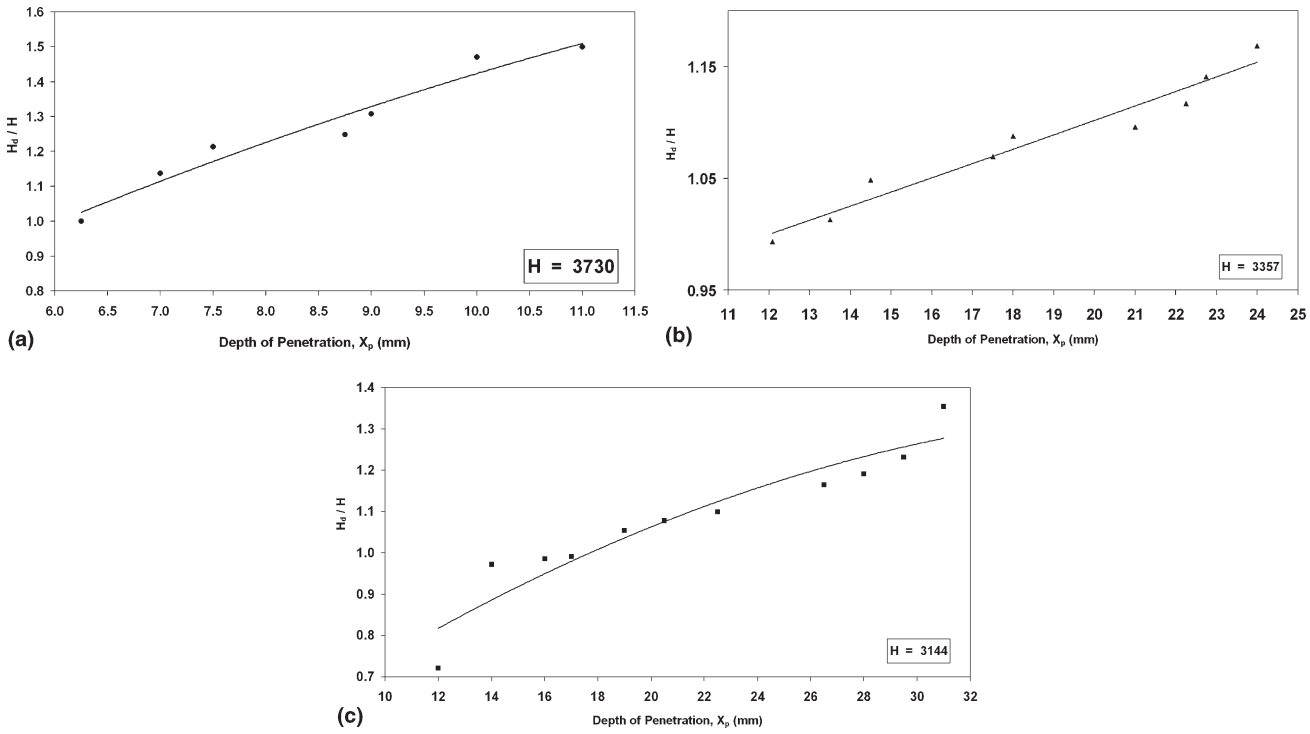

FIG. 6. The variation of normalized dynamic hardness (H_d/H) with depth of penetration (X_p) in the case of (a) 6.2-mm-projectile impacting a 20-mm-thick steel plate, (b) 20-mm-projectile impacting a 40-mm-thick steel plate, and (c) 20-mm-projectile impacting a 8-mm-thick steel plate.

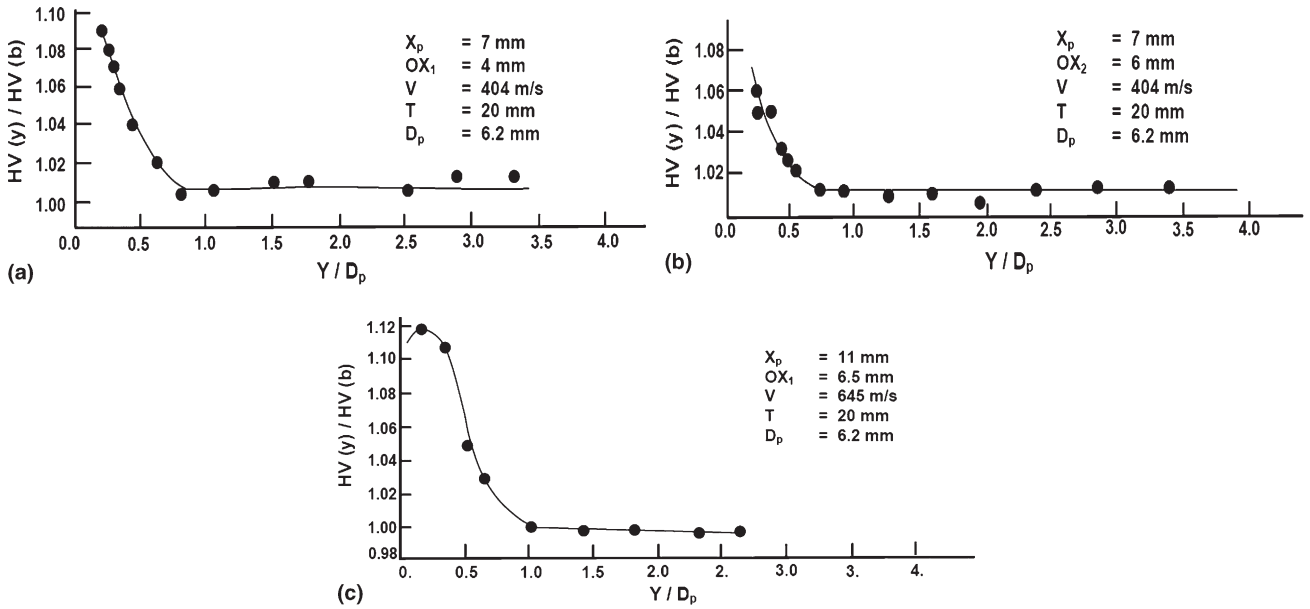

FIG. 7. Microhardness profiles depicting the variation of the normalized microhardness as a function of normalized distance carried out on surfaces obtained by sectioning the indentations formed by 6.2-mm projectile impacting 20-mm-thick steel plate (a) X_p = 7 mm, OX_1 = 4 mm, V = 404 m/s; (b) X_p = 7 mm, OX_2 = 6 mm, V = 404 m/s, and (c) X_p = 11 mm, OX_1 = 6.5 mm, V = 645 m/s.

$$V_b = V/(\alpha^2 - 1) \quad . \tag{4}$$

In Eq. (4), V is the projectile velocity and α is the normalized plastic zone size as defined earlier. However, it should be noted that the projectile velocity (initially at V) decreases continuously during the course of penetration and ultimately reaches a value of zero corresponding to the end of penetration. Therefore, as a first approximation, the average value for V_b (i.e., $V_{b,av}$) can be taken as $V_b/2$. Consequently, the inertial energy consumption (E_{iner}) can be obtained as

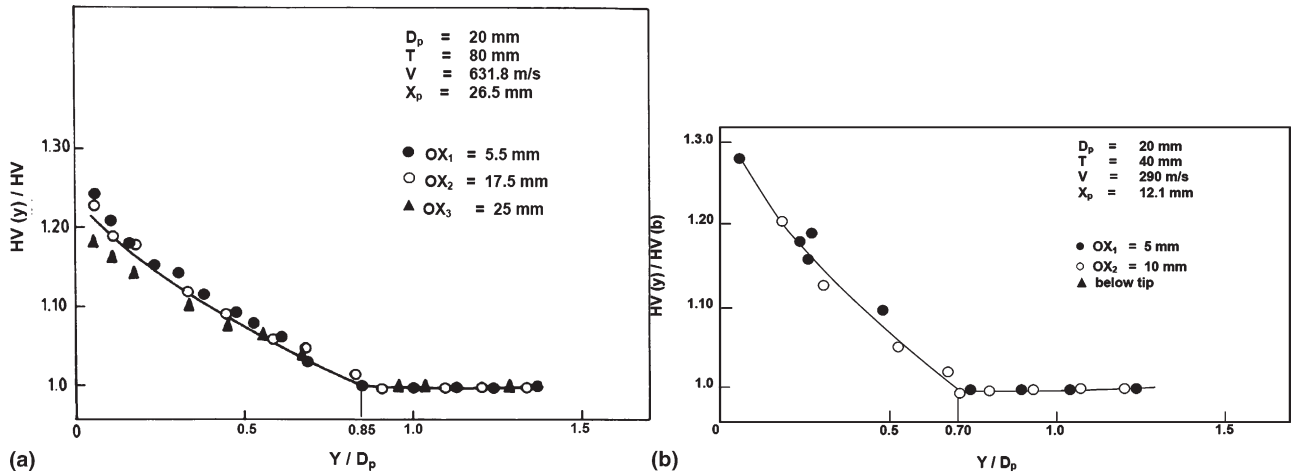

FIG. 8. Microhardness profiles depicting the variation of the normalized microhardness as a function of normalized distance carried out on surfaces obtained by sectioning the indentations formed by 20-mm projectiles impacting the steel plate (a) T = 80 mm, X_p = 26.5 mm, V = 631.8 m/s, and (b) T = 40 mm, X_p = 12.1 mm, V = 290 m/s.

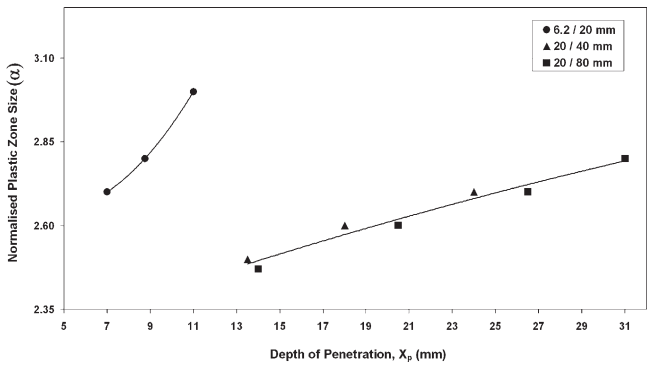

FIG. 9. The variation of the normalized plastic zone size (α) with depth of penetration (X_p) for all combinations of projectile diameter and plate thickness.

$$E_{\text{iner}} = \frac{1}{2}\rho_t \frac{V_{b,av}^2}{(\alpha^2-1)^2} = \frac{1}{8}\rho_t \frac{V^2}{(\alpha^2-1)^2} \quad . \qquad (5)$$

For the typical combinations of impact velocity (V) and the normalized plastic zone size (α) pertinent to the present experiments, E_{iner} is always less than 4% of the input kinetic energy of the projectile and hence can be neglected.

In conclusion, it can be stated that under the experimental conditions of impact velocity and projectile kinetic energy, more than 95% of the input kinetic energy is consumed in the plastic deformation of the steel plate and thus, the indentation is quite similar to that obtained at low penetration depths as in hardness tests.

B. Dynamic hardness and plastic zone size

The normalized dynamic indentation hardness (H_d/H) data presented earlier [Figs. 6(a)–6(c)] can be brought together by normalizing the penetration depth (X_p) by the projectile radius (R), as illustrated in Fig. 10. The

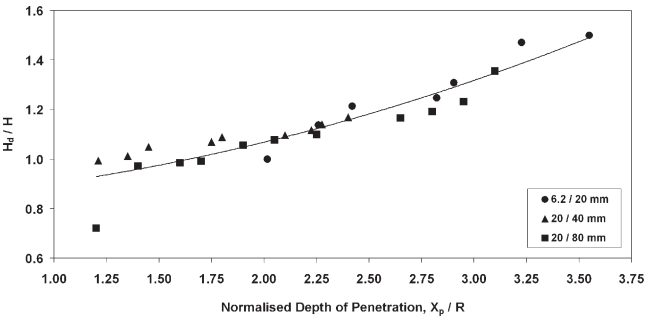

FIG. 10. The variation of normalized dynamic hardness (H_d/H) as a function of the normalized depth of penetration (X_p/R) for all combinations of projectile diameter and plate thickness.

above normalization is effective in merging the dynamic hardness data obtained from all the different indentation tests conducted in the present study. It is clear from Fig. 10 that H_d/H increases continuously with increasing value of X_p/R from a value of around 1 at $X_p/R \simeq 1.25$ to as high as 1.5 at X_p/R = 3.50. The above increase in H_d with increasing penetration can be due to the increase in plastic zone size or an increase in the plastic strain within the plastic zone. These aspects will be considered in greater detail in the subsequent subsections.

The variation of the normalized plastic zone size (α) obtained from all the indentation experiments (Fig. 9) can also be brought together by plotting α against X_p/R as presented in Fig. 11. Once again, all the data merge together and indicate that α increases continuously with increasing value of X_p/R from a low value of around 2.4 to 3.0. It also follows from Figs. 10 and 11 that the H_d value is related to the magnitude of α with a higher α value resulting in a higher hardness. This is clearly brought out in Fig. 12. This is to be expected because the magnitude of α determines very strongly the volume of the plastic zone, as discussed in Sec. IV. C.

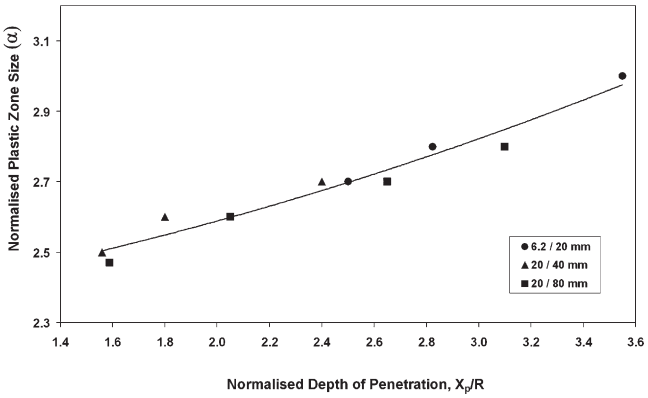

FIG. 11. The variation of normalized plastic zone size (α) as a function of the normalized depth of penetration (X_p/R) for all combinations of projectile diameter and plate thickness.

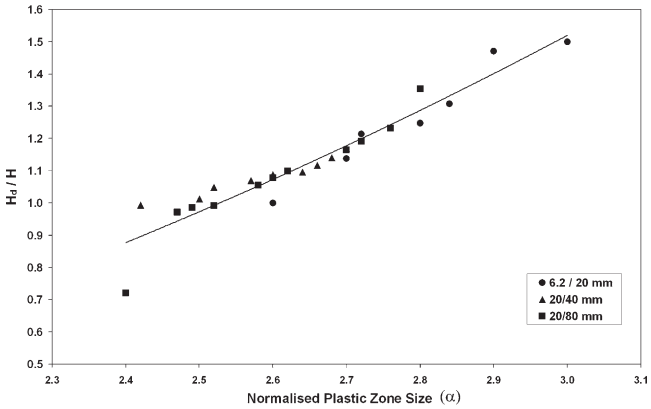

FIG. 12. The variation of dynamic hardness (H_d/H) as a function of the normalized plastic zone size (α) for all combinations of projectile diameter and plate thickness.

C. Plastic zone volume and energy absorption

In Sec. III. C, the shape of the plastic zone was arrived at on the basis of microhardness profiles carried out on sectioned surfaces. Therefore, the volume of the plastic zone (U_{pl}) can be easily computed as

$$U_{pl} = \frac{2}{3}\pi\alpha^3 R_e^3 \quad \left[X_p \le R\right] \quad , \tag{6}$$

$$U_{pl} = \frac{2}{3}\pi\alpha^3 R^3 + \pi R^2\alpha^2\left(X_p - L_N\right) \quad \left[X_p > R\right] \quad . \tag{7}$$

In Eqs. (6) and (7), R_e is the indentation radius when $X_p < R$, R is the projectile radius in its cylindrical portion, and L_N is the nose length of the projectile. The plastic zone volume calculated using Eq. (6) or (7) is presented in Fig. 13(a) as a function of normalized depth of penetration (X_p/R). The plastic zone volume (U_{pl}) generally increases with increasing X_p/R values and is substantially higher for indentations formed with 20-mm-diameter projectile as compared to 6.2-mm projectile. In Fig. 13(b), the plastic zone volume has been normalized by the projectile volume (i.e., U_{pl}/U; U = projectile volume), and it is clear that the plastic zone size is larger than the projectile volume by a factor of 8 to 13; depth of penetration (X_p/R) does not have any discernible influence on U_{pl}/U.

Once the volume of plastic zone (U_{pl}) is known, the specific energy absorption capacity of the steel plate material resulting from plastic deformation (E_{pl}) can be obtained as

$$E_{pl} = \tfrac{1}{2}mV^2/U_{pl} \quad . \tag{8}$$

In Eq. (8) $\tfrac{1}{2}mV^2$ represents the initial kinetic energy of the projectile, which is consumed in the plastic deformation of the steel material within the plastic zone surrounding the projectile.

The variation of the parameter E_{pl} with X_p and X_p/R is presented in Figs. 14(a) and 14(b), respectively. It is clear that the magnitude of E_{pl} lays in the range 275–525 MPa and generally shows an increasing trend with increasing values of X_p/R [see Fig. 14(b)].

The E_{pl} represents the energy consumed per unit volume in plastically deforming the material in the plastic zone up to an average strain ε_{av}. The magnitude of ε_{av} is easily obtained once E_{pl} is known, because E_{pl} is given by

$$E_{pl} = \int_0^{\varepsilon_{av}} \sigma d\varepsilon = \int K.\varepsilon^n\, d\varepsilon = \frac{K.\varepsilon_{av}^{n+1}}{n+1} \quad , \tag{9}$$

ε_{av} is then obtained by rearrangement of Eq. (9) as

$$\varepsilon_{av} = \left(\frac{E_{pl}(n+1)}{K}\right)^{1/n+1} \quad . \tag{10}$$

The values of K and n for the 3 steel plates used in this investigation are given in Table I. The variation of average plastic strain [calculated using Eq. (10)] with X_p and X_p/R are presented in Figs. 15(a) and 15(b), respectively. The calculated ε_{av} values lie in the range 24–40% and more importantly increases with increasing X_p/R values.

D. Dynamic indentation at shallow and large depths of penetration: A comparison

1. Variation of hardness (H_d/H) with penetration (X_p/R)

In the case of fully plastic indentation to shallow depths ($X_p < R$), X_p/R is related to the average plastic strain in the plastic zone through the Tabor relationship.[1] In addition, the normalized plastic zone size (α) is a constant independent of penetration (i.e., X_p/R) and in fact, the applicability of the Tabor relationship for plastic strain requires that α be independent of X_p/R (i.e., ε_{av}). As a result, the increase in hardness at shallow depths is entirely a result of the strain-hardening effects (i.e., $H = H_o\varepsilon_{av}^n$).

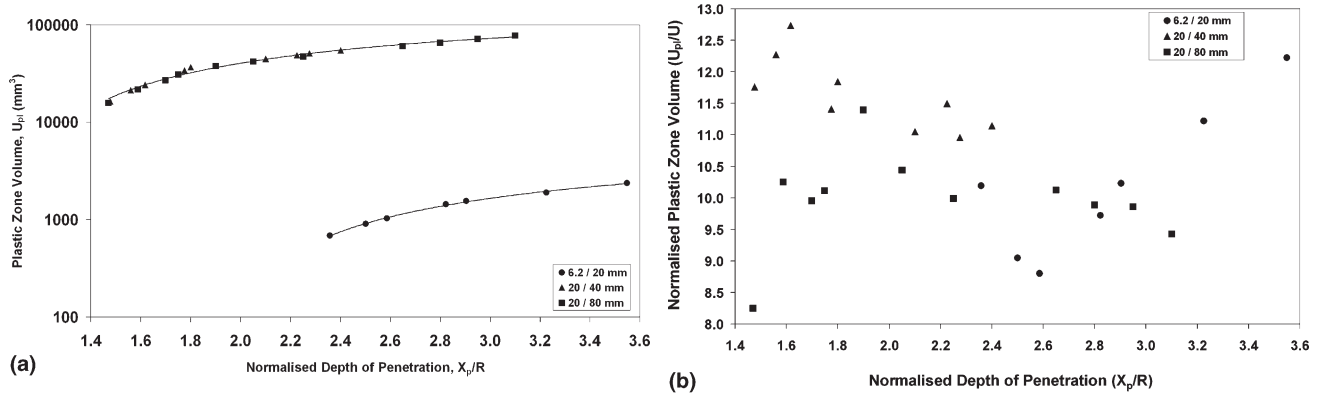

FIG. 13. The variation of (a) plastic zone volume (U_{pl}) and (b) normalized plastic zone volume (U_p/U) as a function of normalized depth of penetration (X_p/R) for all combinations of projectile diameter and plate thickness.

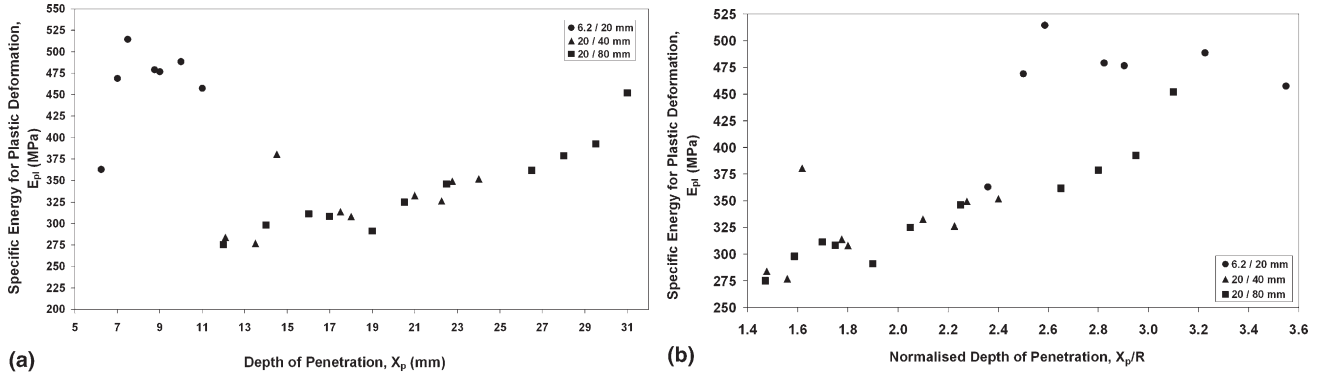

FIG. 14. The variation of specific energy for plastic deformation (E_{pl}) as a function of (a) depth of penetration (X_p) and (b) normalized depth of penetration (X_p/R) for all combinations of projectile diameter and plate thickness.

In contrast, at larger depths of penetration (i.e., $X_p/R > 1$), the Tabor relationship does not apply even though the average plastic strain does increase with increasing X_p/R [see Fig. 15(b)]. However, the increase in plastic strain from an average value of 25–40% [as X_p/R varies from 1.5 to 3.5; Fig. 15(b)] causes an increase in hardness by only 5% (because n values for the steels used in this study are low in the range 0.07–0.1; Table I). In contrast, the experimentally observed increase in hardness is as high as 50% at an X_p/R value of 3.5. Thus, it can be concluded that the increase in the value of α and hence the plastic zone volume with increasing X_p/R (Figs. 9 and 11) is primarily responsible for the observed increase in hardness with X_p/R, as illustrated in Fig. 10.

2. Increase in α with increasing penetration

As discussed in the last section, in the present set of experiments, α is increasing with X_p/R in contrast to a constant value usually expected under fully plastic indentation conditions at shallow depths. If we accept the premise that α increases with X_p/R, it follows then that during a single indentation test α should increase with increasing penetration. This in turn requires that the plastic zone continuously increase in size all the way back to the top surface because the material flow direction is backwards (see Fig. 1). However, such a scenario is not physically possible given the fact that the backward flow velocity of the material displaced by indentation [V_b; Eq. (4)] is always considerably lower than the forward velocity of the projectile [because $\alpha > 1$ in Eq. (4)], and thus there is no time available for the material to traverse all the way back to the top surface. On the other hand, if the plastic zone size remains constant during the penetration process, then the material displaced at the projectile tip has to traverse only a short distance backwards and push the material ahead in an upward direction. Thus, it can be concluded that an increase in α with increasing X_p/R (Fig. 11) is actually a reflection of the effect of increasing initial impact velocity (V).

The question that requires an answer is why α increases with increasing V. The most likely explanation is related to the fact that the inertial energy consumed in moving the plate material away from the path of the

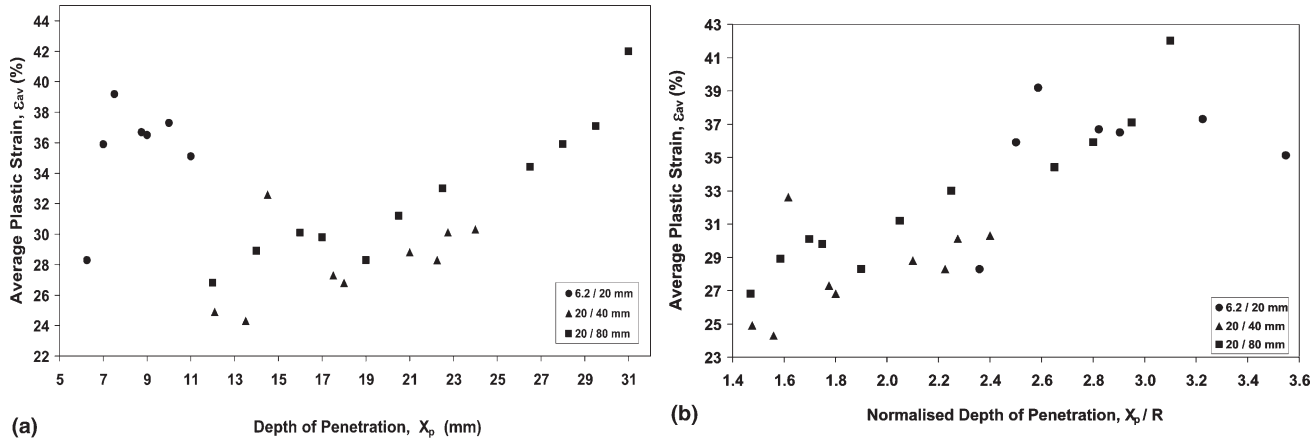

FIG. 15. The variation of average plastic strain (ε_{av}) as a function of (a) depth of penetration (X_p) and (b) normalized depth of penetration (X_p/R) for all combinations of projectile diameter and plate thickness.

projectile, even though negligible when the energy consumed in the whole indentation process is considered (see Sec. IV. A), makes the highest contribution at the start of the indentation process when the projectile velocity is the highest. More importantly, the inertial energy consumption [E_{iner}; Eq. (5)] increases dramatically with decreasing value of α. For example, an increase in the value of α from 2.4 to 3.0 decreases E_{iner} [Eq. (5)] nearly by a factor of 3. It can be then postulated that the value of α increases with increasing impact velocity mainly to offset the increase in inertial energy because of increase in impact velocity thereby maintaining the inertial energy consumption constant and manageable. It also follows that the initial impact velocity determines the magnitude of α, which is then maintained all through the penetration process, resulting in a plastic zone shape consistent with that inferred from the microhardness profile data.

3. Similarity of the indentation process at low and high penetration depths

In Sec. III, the variation of normalized plastic zone volume [U_{pl}/U; Fig. 13(b)], specific energy for plastic deformation [E_{pl}; Fig. 14(b)], and average plastic strain [ε_{av}; Fig. 15(b)] with normalized depth of penetration X_p/R have been presented for large penetration depths ($X_p/R > 1$). It should be instructive to examine whether the values of the previous three parameters (U_{pl}/U, E_{pl}, and ε_{av}) obtained at low penetration depths ($X_p/R < 1$) using spherical balls are in line with the high depth of penetration data. To affect such a comparison, the parameters U_{pl}/U, E_{pl}, and ε_{av} have to be obtained for shallow spherical ball indentation in terms of the normalized depth of penetration (X_p/R). Simple geometrical considerations result in the following expression for U_{pl}/U in the case of spherical ball indentation to shallow depths (i.e., $X_p < R$)

$$\frac{U_{pl}}{U} = \frac{2}{3}\alpha^3 \frac{\left[2(X_p/R) - (X_p/R)^2\right]^{3/2}}{(X_p/R)^2(1 - X_p/3R)} \quad . \tag{11}$$

The average plastic strain (ε_{av}) for shallow spherical indentation is given by the Tabor relation, which when expressed in terms of X_p/R, gives the relation

$$\varepsilon_{av} = 0.2\left[2(X_p/R) - (X_p/R)^2\right]^{1/2} \quad . \tag{12}$$

Finally, the specific energy for plastic deformation (E_{pl}) is given as

$$E_{pl} = \int_O^{\varepsilon_{av}} K\varepsilon^n d\varepsilon = \frac{K\varepsilon_{av}^{n+1}}{n+1} \quad . \tag{13}$$

In Eq. (13), ε_{av} is obtained using Eq. (12).

The values of U_{pl}/U, ε_{av}, and E_{pl} calculated as a function of X_p/R using Eqs. (11), (12), and (13) are presented in Figs. 16(a), 16(b), and 16(c), respectively, along with the data pertinent to $X_p/R > 1$. In each of these figures, the filled points indicate high penetration depth data, whereas the unfilled points pertain to shallow depth spherical indentation. It is obvious from Fig. 16 that all the three parameters (i.e., U_{pl}/U, E_{pl}, and ε_{av}) show continuity over the whole range of penetration (i.e., low as well as high depths of penetration). On the above basis, it can be concluded that the indentation process under fully plastic conditions is the same irrespective of the depth of penetration.

4. Relationship between E_{av} and X_p/R

At low penetration depths with spherical ball, the average strain in the plastic zone (ε_{av}) is described by the Tabor relation, given by Eq. (12). For $X_p/R < 0.4$, Eq. (12) can be approximated by Eq. (14) given below

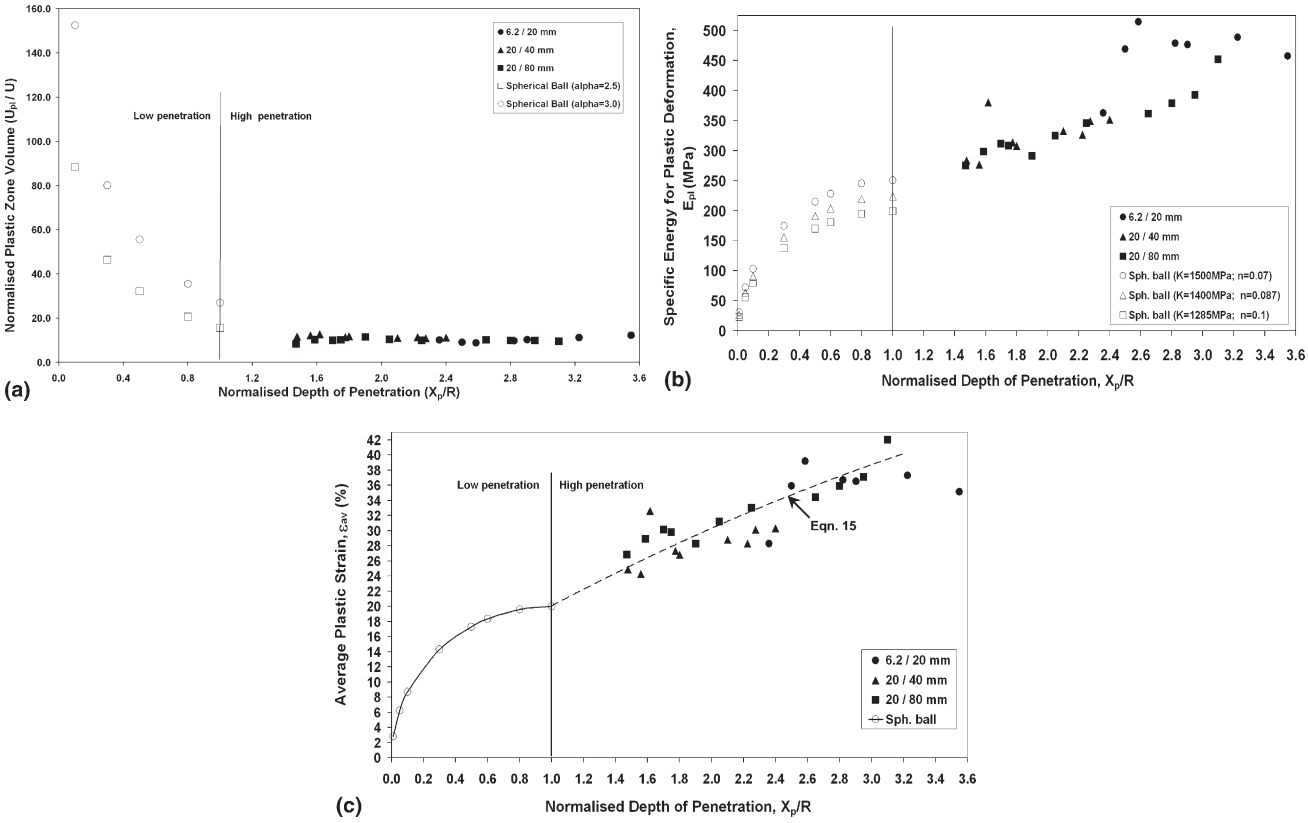

FIG. 16. Variation of (a) normalized plastic zone volume (U_{pl}/U), (b) specific energy for plastic deformation (E_{pl}), and (c) average plastic strain (ε_{av}) as a function of normalized depth of penetration (X_p/R) over the whole range of penetration depths. The figure includes the low penetration depth data (unfilled symbols) obtained using spherical ball indentors and the high penetration depth data (filled symbols) obtained with ogive projectiles.

$$\varepsilon_{av} \simeq 0.283\left(X_p/R\right)^{1/2} \quad . \tag{14}$$

Thus, at very low penetration depths, ε_{av} scales as $(X_p/R)^{1/2}$. To see whether a similar relationship holds for high penetration data ($X_p/R > 1$), the data points valid for $X_p/R > 1$ were fitted to an equation similar to Eq. (14), and the best-fit equation [see the dashed line in Fig. 16(c) for the extent of the fit] was obtained as,

$$\varepsilon_{av} = 0.2\left(X_p/R\right)^{0.6} \quad \left[\text{for } X_p/R > 1\right] \quad . \tag{15}$$

Thus, ε_{av} scales as $(X_p/R)^{0.6}$ at larger penetration depths. It is also interesting to note that at $X_p/R = 1$, both Eq. (15), valid for higher penetration depths and the Tabor relation [Eq. (12)], valid for shallow penetration, give the same value of 20% for ε_{av} pointing to the continuity in the ε_{av} values across the complete penetration regime. The physical basis for the scaling law observed above is not clear and requires further analysis.

V. CONCLUSIONS

The major conclusions from the present study are as follows.

(1) The hardness of the steel plate increases with increasing penetration (i.e., X_p/R), and this is primarily related to the fact that the plastic zone volume (related to α) increases with increasing penetration. This is in contrast to shallow penetration with spherical balls (at impact velocities lower than that used in the present study), wherein the hardness increase with increasing X_p/R is fully accounted for by strain-hardening effects because X_p/R is related to ε_{av} in the plastic zone through the Tabor relationship.

(2) The normalized plastic zone size (α) increases with increasing initial impact velocity in contrast to shallow penetration with spherical balls (at impact velocities lower than that used in the present study), wherein α is a constant independent of X_p/R and hence initial impact velocity.

(3) The average strain (ε_{av}) in the plastic zone scales as $(X_p/R)^{0.6}$ in the high penetration regime; whereas in the low penetration regime ε_{av} scales as $(X_p/R)^{0.5}$.

(4) The indentation process is identical irrespective of depth of penetration and the kinetic energy of the projectile is mostly consumed through the plastic deformation of the steel material within the plastic zone surrounding the penetrating projectile. As a result, important indentation related parameters like normalized plastic zone size, the specific energy for plastic deformation, and the average plastic strain vary smoothly and continuously over the whole range of penetration depth irrespective of whether the penetration depth is lower or higher than projectile radius.

REFERENCES

1. D. Tabor: *The Hardness of Metals* (Oxford University Press, UK, 1951).
2. C.H. Mok and J. Duffy: The dynamic stress-strain relation of metals as determined from impact tests with a hard ball. *Int. J. Mech. Sci.* **7,** 355 (1965).
3. G. Sundararajan and P.G. Shewmon: The use of dynamic impact experiments in the determination of the strain rate sensitivity of metals and alloys. *Acta Metall.* **31,** 101 (1983).
4. Y. Tirupataiah and G. Sundararajan: A dynamic indentation technique for the characterization of high strain rate flow behavior of ductile materials. *J. Mech. Phys. Solids* **39,** 243 (1991).
5. G. Subhash, B.J. Koeppel, and A. Chandra: Dynamic indentation hardness and rate sensitivity in metals. *J. Eng. Mater. Technol.* **121,** 257 (1999).
6. B.J. Koeppel and G. Subhash: Characteristics of residual plastic zone under static and dynamic Vickers indentation. *Wear* **224,** 56 (1999).
7. G. Sundararajan and Y. Tirupataiah: The localization of plastic flow during dynamic indentation. I: Experimental results. *Acta Mater.* **54,** 565 (2006).
8. G. Sundararajan and Y. Tirupataiah: The localization of plastic flow during dynamic indentation. II: Analysis of results. *Acta Mater.* **54,** 577 (2006).
9. R.B. Clough, S.C. Webb, and R.W. Armstrong: Dynamic hardness measurements using a dropped ball—With application to 1018 steel. *Mater. Sci. Eng., A* **360,** 396 (2003).
10. S.N. Dikshit, V.V. Kutumba Rao, and G. Sundararajan: The influence of plate hardness on the ballistic penetration of thick steel plates. *Int. J. Impact Eng.* **16,** 293 (1995).
11. S.N. Dikshit: A comprehensive analysis of the ballistic penetration of high kinetic energy projectiles into steels: Experiment and modelling. Ph.D. Thesis, Defence Metallurgical Research Laboratory, Hyderabad, India, 1996.
12. S.N. Dikshit and G. Sundararajan: The penetration of thick steel plates by ogive shaped projectiles: Experiment and analysis. *Int. J. Impact Eng.* **12,** 373 (1992).